Marine Geology, 56 (1984) 119—136
Elsevier Science Publishers B.V., Amsterdam — Printed in The Netherlands

HIGH RESOLUTION STRATIGRAPHIC CORRELATION OF BENTHIC OXYGEN ISOTOPIC RECORDS SPANNING THE LAST 300,000 YEARS

N.G. PISIAS[1], D.G. MARTINSON[2], T.C. MOORE, Jr.[3], N.J. SHACKLETON[4], W. PRELL[5], J. HAYS[6] and G. BODEN[7]

[1] *School of Oceanography, Oregon State University, Corvallis, OR 97331 (U.S.A.)*
[2] *Woods Hole Oceanographic Institution, Woods Hole, MA 02543 (U.S.A.)*
[3] *Exxon Production Research, Houston, TX 77001 (U.S.A.)*
[4] *Sub-Department of Quaternary Research, The Godwin Laboratory, Free School Lane, Cambridge, CB2 3RS (Great Britain)*
[5] *Department of Geological Sciences, Brown University, Providence, RI 02912 (U.S.A.)*
[6] *Lamont Doherty Geological Observatory, Palisades, NY 10964 (U.S.A.)*
[7] *Graduate School of Oceanography, University of Rhode Island, Kingston, RI 02881 (U.S.A.)*

(Received April 13, 1983; revised and accepted June 24, 1983)

ABSTRACT

Pisias, N.G., Martinson, D.G., Moore Jr., T.C., Shackleton, N.J., Prell, W., Hays, J. and Boden, G., 1984. High resolution stratigraphic correlation of benthic oxygen isotopic records spanning the last 300,000 years. Mar. Geol., 56: 119—136.

In order to compare the response of different oceanographic regions to global climate change, very detailed stratigraphic techniques are required. The global signal of ice volume changes recorded in the oxygen isotopic composition of foraminifera can provide the tool for developing the necessary high resolution stratigraphy. In order to evaluate the resolution of a stratigraphy based on detailed isotopic records, two techniques are used to correlate a set of benthic oxygen isotope records from seven piston cores taken in the North and South Atlantic, the Indian, and the equatorial and North Pacific oceans.

The first technique was modified from the graphic correlation procedure of Shaw (1964). This procedure requires the identification of isotopic events that are correlated from core to core. Detailed correlations for intervals of the cores between events are provided by a series of straight line segments connecting all common events. The second technique developed by Martinson et al. (1982) uses inverse procedures to define a continuous non-linear mapping function that correlates the isotopic records. The mapping function maximizes the correlation coefficient between data sets being compared. The techniques are independent in that they rely on different criteria for correlating the data series.

Stratigraphic correlations obtained by these procedures are in excellent agreement. The mean difference between the correlations is on the order of the sampling intervals of each core and, when corrected for sedimentation rates, suggests that benthic isotope records from the suite of seven cores can be correlated to a resolution of 2000 to 4000 yrs.

0025-3227/84/$03.00

INTRODUCTION

The reconstruction of the glacial ocean (CLIMAP, 1976, 1981) required that investigators identify the last glacial maximum in a global array of deep-sea sediment cores. The development of oxygen isotopic stratigraphy (Emiliani, 1955; Shackleton and Opdyke, 1973; Shackleton, 1977) made this task possible. Variation in the isotopic composition of the ocean as measured in foraminiferal tests is controlled primarily by the amount of water stored as land ice (Shackleton and Opdyke, 1973). Within the mixing time of the ocean, variations in the oxygen isotopic record measured in sediment cores should provide a globally synchronous stratigraphy. Radiometric ages from sediment cores with isotopic measurements give a mean age for the last glacial ice maximum of 18,000 yrs with a standard deviation of 1300 yrs (Pisias, 1976). This spread in radiometric ages is consistent with estimates of oceanic mixing times ($\leqslant$1000 yrs) and supports the assumption that variations in the oxygen isotopic record are synchronous in ocean sediments.

On a long-time scale ($\geqslant 10^5$ yrs) the degree of similarity in isotopic records from deep-sea sediments has resulted in the definition of isotopic stages for the late Pleistocene (Emiliani, 1955; Shackleton and Opdyke, 1973). On a shorter time scale, isotopic stage 5 has been subdivided into substages 5a and 5e which have been correlated to sea level changes evidenced in exposed reef deposits (Mesolella et al., 1969). These changes in sea level and the associated isotopic response occur on time intervals of about 20,000 yrs and suggest that the isotopic record provides stratigraphic resolution of less than 20,000 yrs.

In this study, a high resolution stratigraphy is developed for oxygen isotopic records of deep-sea sediment cores that span the last 300,000 yrs and have a sampling resolution of about 500 yrs. This stratigraphy is based on the assumptions that an oxygen isotopic record measured in a sediment core documents changes in global ice volume and that variations in the isotopic composition of the world's ocean are synchronous within the mixing time of the ocean.

DATA

The oxygen isotopic data used in this study come from seven sediment cores which appear to have relatively continuous, undisturbed sedimentation (Table I). Because we wish to study oceanographic and climatic change on a time scale of a few thousand years, only cores with relatively high sedimentation rates were selected. In the cores used, the sedimentation rates range from 2.2 to 10 cm per 1000 yrs or greater. The cores are from all major oceans, with three from the eastern equatorial Pacific, and one each from the northeast Pacific, eastern South Atlantic, eastern tropical North Atlantic, and the northwestern Indian Oceans. All analyses (Fig.1) were made on the benthic foraminifera genus *Uvigerina* with the exception of the Indian Ocean core

TABLE I

Core locations and sedimentation rates

Core No.	Ocean	Lat.	Long.	Water depth (m)	Record length (cm)	No. of points	Average sampling interval (cm)	Mid-value for scaling	Average sediment rate (cm 1000 yrs^{-1})
V19-29	P	3°35'S	83°56'W	3157	1680	179	9.4	4.06	5.6
V19-28	P	2°22'S	84°39'W	2720	1618	140	11.6	4.13	3.8
V19-30	P	3°23'S	83°31'W	3091	850	258	3.3	4.30	6.4
Y7211-2	P	43°15'N	126°23'W	3000	1570*	203	7.2	4.11	10.2
MD76-135	I	14°27'N	50°31'E	1895	960	96	10.0	3.15	6.9
M12392	A	25°10'N	16°50'E	2573	950	95	10.0	4.15	6.6
RC13-229	A	25°30'S	11°18'E	4191	1632	151	10.8	4.11	2.2

*30—1600 cm.

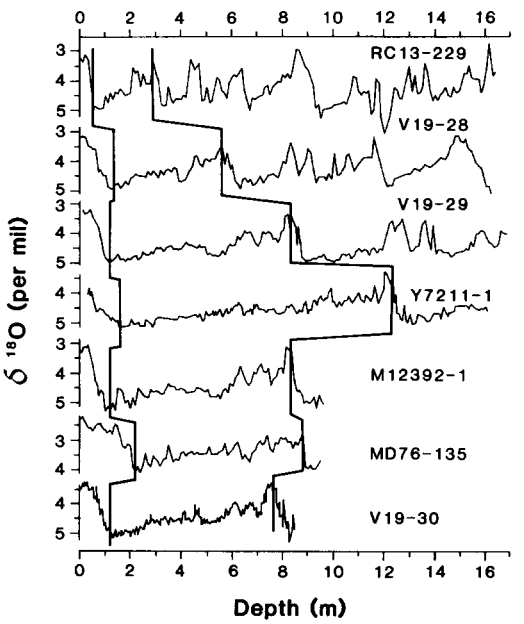

Fig.1. Oxygen isotopic records used in detailed correlations. All cores plotted versus original depth in sediments. Horizontal lines mark last glacial maximum (stage 1) and last full interglacial (stage 5e).

where specimens of *Cibicides* were analyzed (Table I). The data are presented relative to PDB standard calcite. Benthic foraminiferal data were used in this study to reduce the effects of temperature and/or salinity on changes in the isotopic records. However, variations in "bottom" water conditions at the core site M12392 have superimposed a significant non-ice volume signal on this record (Shackleton et al., 1983).

STRATIGRAPHIC METHODS

Two different strategies were used to provide detailed correlations between the seven cores studied. The first strategy is essentially the graphical correlation technique of Shaw (1967) with modifications as outlined by Prell et al. (1983). The second is the inverse correlation technique of Martinson et al. (1982). The goal of both approaches is to define a mapping function which converts the depth units in each of the individual cores to units of depth in a standard section. The first strategy utilizes the presence of discrete event to correlate sediment sections whereas inverse correlation provides a continuous function correlating two data sets. These techniques are independent approaches to correlation which are applied to the same data sets. The differences between the correlations provide some measure of the resolution possible.

Graphical correlations

The graphical correlation technique requires the identification of unique events which can be identified (ideally) in all the isotopic records being studied; however, one of its advantages is that it does not require that all events occur in all cores. To facilitate the identification of events, the isotopic records of all cores were plotted so that the distance between the last glacial maximum and the last full interglacial (isotope substage 5e) was constant. The principle isotopic stage boundaries of Emiliani (1955) and substages of isotope stage 5 were identified where possible. Within these stages additional isotopic events (times of depleted or enriched values) were noted. In this detailed selection of events, only features which (a) could be identified in more than one core; (b) were characterized by more than one point peaks (or valleys); and (c) represented change in isotopic values at least equal to analytic precision ($\sim 0.1^{\circ}/_{oo}$ ΔO^{18}), were considered to be of stratigraphic importance.

A numbering convention was used to label the isotopic events which follows the numerical isotope taxonomy of Prell et al. (1983). The integer portion of the event number gives the isotopic stage in which the event occurs, the first digit to the right of the decimal point gives the substage event identified by Prell et al. (1983) in isotopic records spanning the last 700,000 yrs and for the most part having sedimentation rates on the order of 2 cm per 1000 yrs. The digit in the second decimal place represents events identified in this study of high sedimentation rate cores. The convention of using even numbers to represent enriched intervals and odd numbers to represent depleted intervals is followed for all stages and substages. For example, the event 3.1 is the youngest depleted value in isotope stage 3 identified in low resolution cores by Prell et al. (1983) and 3.13 is a depleted event older than event 3.1 but younger than event 3.3 seen in the benthic records of this study (Figs.1 and 2). Isotopic stage boundaries are listed as whole numbers. A "taxonomy" of these events is given in Table II and is

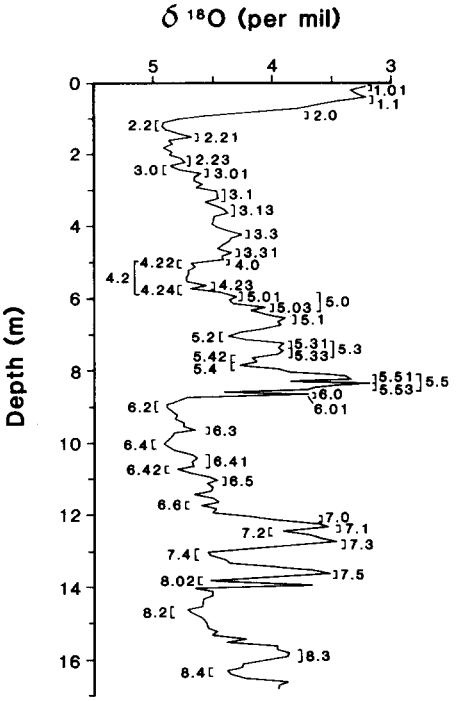

Fig.2. Isotopic events as picked in the record from core V19-29. Event definition given in Table II.

TABLE II

Isotope taxonomy

Event	Lower depth (cm)	Upper depth (cm)	Comments
1.01	10	0	Youngest negative peak in core; often missing
1.1*	16	11	Most negative peak in stage 1 if core top has not been lost
2.0*	89	70	Boundary between stage 1 and stage 2
2.01	93	82	Minor peak of short duration in high-resolution cores; midway up termination I
2.2*	135	123	Most positive valley in stage 2; close to base of termination I
2.21*	152	140	Younger of two stage 2 peaks in high-resolution cores; about 0.2°/₀₀ difference from event 2.2
2.23*	222	215	Younger stage 2 peak in high-resolution cores; located near the base of the stage; magnitude less than event 2.21
3.0*	242	233	Boundary between stage 2 and stage 3; a rapid depletion of approximately 0.3 to 0.5°/₀₀
3.01	260	248	Youngest of five minor peaks in stage 3 with a height of about 0.15°/₀₀; located near event 3.0 on stage 2/3 transition. This and other peaks in the stage are difficult to resolve even in high-resolution cores

TABLE II (*continued*)

Event	Lower depth (cm)	Upper depth (cm)	Comments
3.1*	308	305	Second minor peak near top of stage 3; about 0.1‰ more negative than event 3.01; in high-resolution cores it may be less well defined
3.13*	361	358	Middle minor peak of stage 3; about 0.2‰ more negative than event 3.1
3.3*	427	419	Next to oldest minor peak; usually the best-defined and most negative peak in the stage
3.31*	473	465	Oldest minor peak of stage; may appear more negative than event 3.3 in some cores, but is located just about stage 3/4 transition
4.0*	498	491	Boundary between stage 3 and stage 4
4.2	561	507	Complete stage 4 in lower-resolution cores, not just most positive value
4.22*	502	498	Youngest valley in stage 4; located at base of stage 3/4 transition; usually about 0.5‰ heavier than event 3.31
4.23*	565	555	Minor peak near base of stage in high-resolution cores; about 0.2‰ lighter than event 4.22
4.24*	573	567	Oldest valley in stage; located at top of stage 4/5 transition; lighter than event 4.22 in high-resolution cores
5.0*	610	590	Boundary between stage 4 and stage 5
5.01	596	585	Youngest of two minor peaks on the transition between stages 4 and 5
5.03	617	615	Older minor peak on transition
5.1*	654	647	Youngest major peak in stage 5; equivalent to the most negative value in substage 5a
5.2*	702	695	Valley separating events 5.1 and 5.3; equivalent to most positive value in substage 5b
5.3*	749	716	Central major peak in stage; less negative than events 5.1 and 5.3 and not as easily defined in high-resolution cores; divided into two minor peaks. Equivalent to substage 5c
5.31*	728	719	Younger minor peak of event 5.3 in higher resolution cores
5.33*	749	739	Older minor peak of event 5.3 and separated from it by a valley up to 0.15‰ deep
5.4*	784	760	Major valley between events 5.3 and 5.5
5.42	766	760	In high-resolution cores, younger of two minor valleys composing event 5.4
5.44	784	775	Older minor valley; not always distinguishable from event 5.42 and it is unclear which is more positive
5.48	808	801	Minor valley of short duration mid-way between events 5.4 and 5.5. In V19-30, 0.3‰ heavier than values on either side
5.5*	840	825	Oldest major peak in stage 5 and isotopically lightest with a value similar to event 1.1; composed of two minor peaks in high-resolution cores. Equivalent to most negative value in substage 5e
5.51*	817	812	Younger minor peak; separated from event 5.53 by a valley of about 0.4‰
5.53*	839	833	Older minor peak; possibly more negative than event 5.51 by up to 0.1‰

TABLE II (*continued*)

Event	Lower depth (cm)	Upper depth (cm)	Comments
6.0*	865	840	Boundary between stage 5 and stage 6
6.01	860	850	Negative event of short duration mid-way through termination II
6.2*	906	896	Youngest of four valleys in stage 6; located at base of stage 5/6 transition
6.3*	968	950	Peak in upper section of stage 6 located between events 6.2 and 6.4; about 0.3°/₀₀ lighter than surrounding valleys
6.4*	1000	1010	Centrally located and usually most positive valley in stage
6.41*	1052	1030	Middle peak in stage; generally less negative than events 6.3 and 6.5
6.42*	1078	1060	Minor valley separating events 6.41 and 6.5; about 0.2°/₀₀ deep
6.5*	1118	1113	Oldest, broad negative peak in stage 6
6.6*	1180	1160	Oldest valley in stage, but lighter than events 6.2, 6.4, or 6.42; located just above stage 6/7 transition
7.0*	1220	1180	Boundary between stage 6 and stage 7
7.1*	1240	1220	Upper peak in stage 7; appears to be slightly heavier than event 7.3 by 0.1°/₀₀
7.2*	1250	1230	Valley separating peaks in upper section of stage; about 0.5°/₀₀ heavier than events 7.1 and 7.3
7.3*	1280	1260	Middle peak in stage; can be taken for event 7.1 in low-resolution cores
7.4*	1305	1290	Most positive value in stage 7; clearly defines upper and lower sections of the stage
7.5*	1365	1350	Oldest peak in stage; less negative than event 7.3
8.0*	1365	1375	Boundary between stage 7 and stage 8
8.02*	1390	1370	Very positive, short-duration event at the base of the stage 7/8 transition
8.2*	1470	1450	Most positive event in stage 8; located in upper section
8.3*	1600	1572	Peak in lower section of stage 8; most negative value is approximately equivalent to magnitude of event 5.3
8.4	1640	1620	Middle valley in stage; less positive than event 8.2

*Events which appear in the composite isotope record (Fig.9).

based on the identification of events in the isotope record from the core used as the standard section, V19-29 (Fig.2). Core V19-29 was used as the standard because of the length and detail of its isotopic record.

The location of each event in a core is not given as a discrete depth but rather as an interval which reflects the sampling spacing in the core. For example, the boundary between the isotope stages 1 and 2 can be defined as the depth in a core where the isotopic composition is the midpoint between the extreme glacial value at the end of stage 2 and the extreme interglacial value of stage 1. As illustrated in Fig.2, the exact position of this transition may not be represented by an actual sample; but rather the position of this event is constrained to be within a depth range defined by real sample values. Similarly the location of an isotopic maximum is the depth range defined by half the distance to the samples on either side of the one with the measured

maximum value. Correlations between all cores and the standard section are defined by straight line segments drawn through the correlation "boxes" formed by the depth range of resolution for each event in the core records (Prell et al., 1983). Line segments were drawn by eye to pass through the maximum number of event boxes (Fig.3). Changes in slope between line segments can be interpreted as representing changes in sedimentation rate in one core relative to the other, or may reflect coring disturbance during the actual sampling of the sediment (Shaw, 1967; Prell et al., 1983). The correlation lines allow the projection of all events into the standard section, even those which do not occur in the standard core. They can also be used to project the estimated ranges of each event in a core into the standard section. The projection of event 2.2 from all cores studied onto the standard core is shown in Fig.4. The interval common to all these range estimates (Fig.4, 128 cm to 135 cm) is considered to be the best estimate of the true position of event 2.2 in the standard section. Similarly, a more constrained estimate of the true position of this event can be made for all other cores by the graphical correlation technique. Diagrams such as Fig.4 were drawn for all events listed in Table II to insure that the projected depth intervals for each core overlapped to form a constrained estimate of the actual depth in the standard section. The true position of each event in a core was then taken as the midpoint values of these "constrained" intervals. Once the midpoints were defined by the graphic correlation technique, every sample in a core was given a depth value equivalent to its estimated depth in the standard section. These estimated (standard depth units) depths are based on linear interpolation between isotopic events. By this technique a correlation to the standard core is made for every sample in each core. When a time scale is

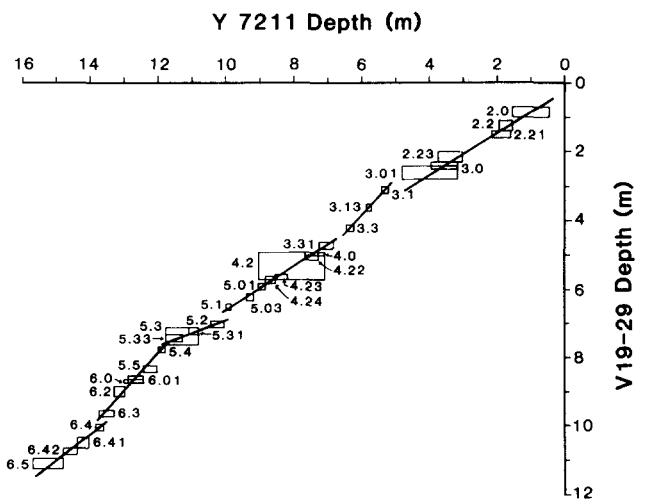

Fig.3. Graphic correlation plot between cores Y7211 and standard core V19-29. Boxes show the depth ranges where the labeled events occur in each core. Straight line segments are drawn to include as many event boxes as possible.

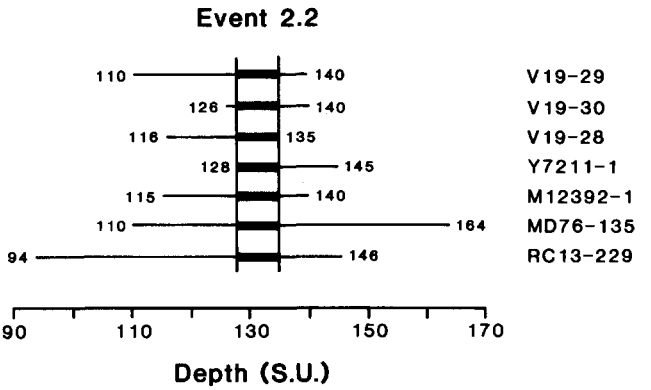

Fig.4. Results of graphic correlations for event 2.2. For core V19-29 the depth range for the event is plotted at top (110 cm to 140 cm). Intervals shown for each core correlated to V19-29 are the predicted intervals for event 2.2 in core V19-29 mode from regression line as shown in Fig.3. The heavy line (the interval of overlap from all correlation lines) represents the best estimate of the position of event 2.2 in the standard core (V19-29).

defined for this standard section, then the samples from all cores could be easily placed into the identical time reference framework.

Inverse correlation

Inverse correlation uses mathematical inverse methods to correlate two data series. If the two series are designated as $D(x)$ and $R(t)$, the technique defines a mapping function $x(t)$ so that the correlation coefficient between the data sets is maximum. In Fig.5, $R(t)$ is the standard signal in which all

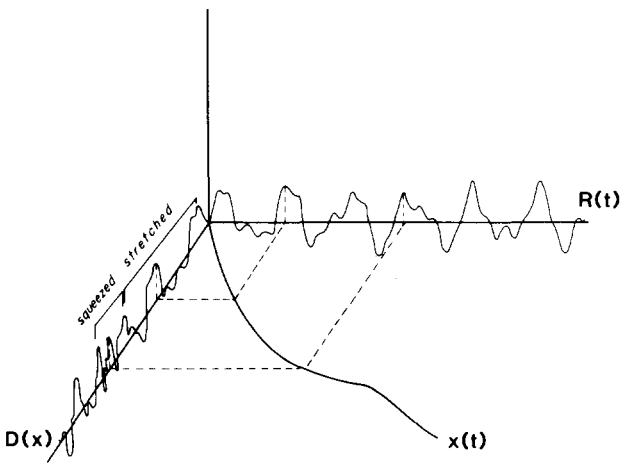

Fig.5. The standard or reference signal, $R(t)$ is related to the distorted signal $D(t)$ through the distorting or mapping function, $x(t)$. When $dx/dt > 1$ the signal is stretched, when $dx/dt < 1$ it is squeezed or compressed.

other core records are to be correlated. The data series $D(x)$ is assumed to be a distorted version of $R(t)$ where the distortion involves stretching and squeezing along the x-axis (depth axis). The mapping function, $x(t)$ equates depth units in series D to depth units in series R and is parameterized in terms of simple functions (in this case, sine functions) weighted by unknown coefficients whose values are selected to maximize the correlation coefficient between the two data series.

Because the technique requires the calculation of the correlation coefficient between the data sets, the procedure must interpolate each data series after a mapping function is determined so that the appropriate cross product terms can be calculated. Also, the convergence to the true maximum in the correlation coefficient can be enhanced if the frequency resolution of the two data series is equivalent. A complete discussion of the technique is given by Martinson et al. (1982) and Martinson (1982).

The inverse technique has two important advantages over graphic correlation in that it is much less time consuming (if a computer is available that can execute the program code required) and the correlations are less subjective as compared to graphical correlations. The graphic correlation procedure, however, has the advantage that it examines all cores for consistent features (the inverse technique operates on only two records at a time); it has the potential of correlation at an extremely fine scale (this is true for inverse techniques if the number of coefficients in the mapping function is allowed to be very large); and the graphic correlation technique uses only information at the actual data position (the inverse correlation must interpolate values to an equal spacing). A potential problem of the inverse technique is that local maxima in the correlation coefficient as a function of the mapping coefficients can cause a convergence to an incorrect solution. Also, the use of a trigonometric expression for the mapping function can introduce "artificial wiggliness" in the mapping function (Shure and Chave, 1983). However, careful application of the technique will usually avoid this problem (Martinson et al., 1982).

The inverse technique was applied to the same seven isotope records used for graphical correlations and, as before, V19-29 was used as the reference signal. This core, originally sampled at 10-cm intervals, was interpolated to 5 cm yielding about 320 values. All other cores were interpolated to 2.5-cm intervals. This interpolation assures the minimal loss of information during the inverse computations. The correlations were initiated using a minimum number of initial stratigraphic correlation control points. In the case of short signals which spanned only one major glacial cycle, an initial guess consisting of a linear trend connecting the end points was usually sufficient. For core MD76-135 an additional stratigraphic correlation point near the center of the record was required. The inverse calculations were initiated using a mapping function with three coefficients. The number of coefficients was then expanded to a total of 30 in steps of two so that local maxima in the correlation coefficient as a function of the mapping function were avoided (Martinson et al., 1982). Although many of the cores contained isotopic

variations at higher frequencies than could be resolved by the standard core V19-29, pre-filtering was required only in case of core Y7211 which contains the highest frequency information of all cores studied (cf. Fig.1). Here we used a low pass filter with a cutoff frequency of 0.45 radian cm^{-1} (the nyquist was 1.05 radians cm^{-1}). The cutoff frequency was iteratively increased following each convergence of the mapping function until 21 mapping coefficients were obtained. Unfiltered data were used in the remaining iterations to the 30 coefficient mapping functions. The mapping functions between core V19-29 and cores V19-28 and V19-30 are shown in Fig.6. Excellent correlations were achieved despite minor differences in the isotope records from these cores.

DISCUSSION

The ultimate goal of both of these stratigraphic correlation techniques is to place a group of sediment cores into a standard depth reference frame. Thus, each sample in a core could be assigned a depth value in the standard section. These standard depth units for each sample in each core are available from the senior author.

Comparison of graphical and inverse correlation techniques

The comparison between the two methods of correlations can be made by directly overlying the event boxes of the graphic correlation technique and its corresponding linear slopes with the recovered mapping functions of

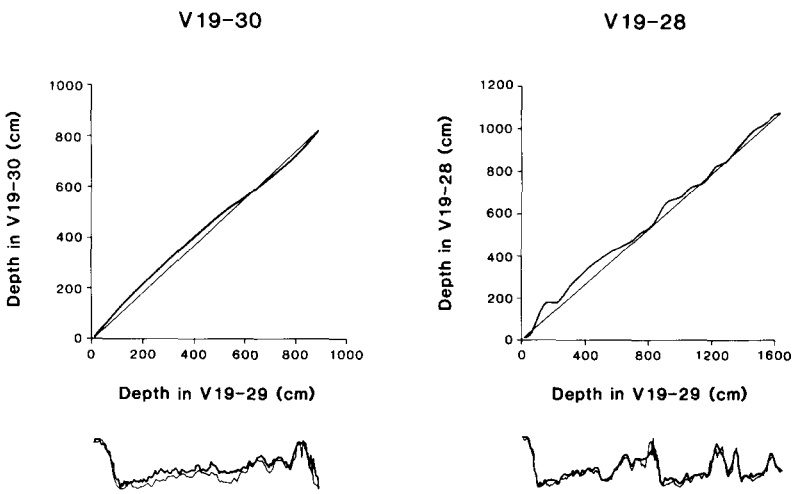

Fig.6. Recovered mapping functions (upper) with straight slope segments showing initial guess relating indicated record to that of V19-29. Lower portion shows correlation results (slightly offset to aid comparison but masks slight amplitude problems) with correlated signal (bold) and V19-29 (light).

the inverse correlation. These comparisons are shown in Fig.7. The two techniques show excellent agreement in the correlations involving cores V19-30, V19-28, RC13-229 and Y7211. For the most part even the fine scale substage structure agrees. This is quite encouraging given the small amplitude of these features and independence of the approaches.

The results are not so agreeable for the Atlantic core M12392 and Indian Ocean core MD76-135. In these two cores the divergence is caused by

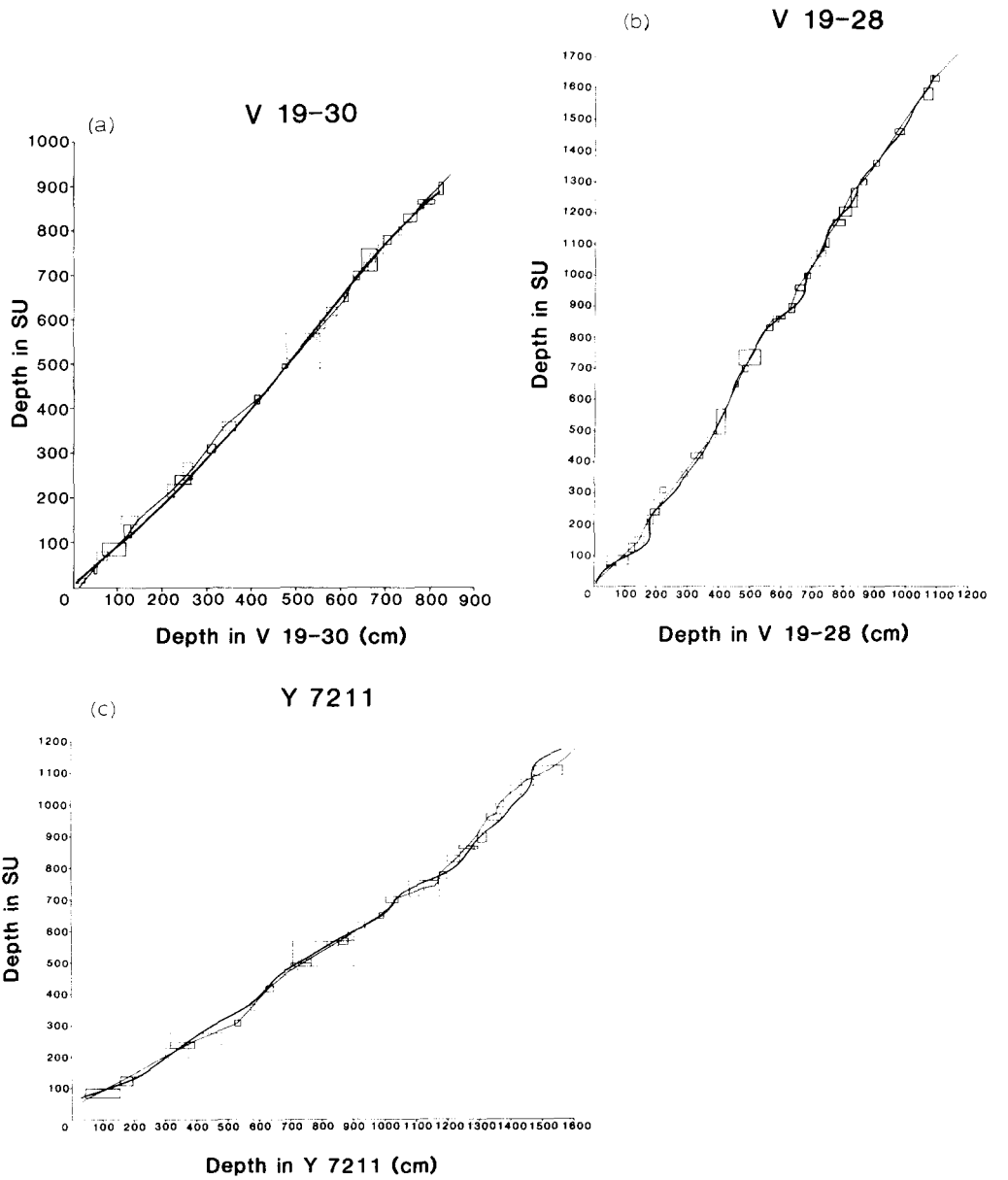

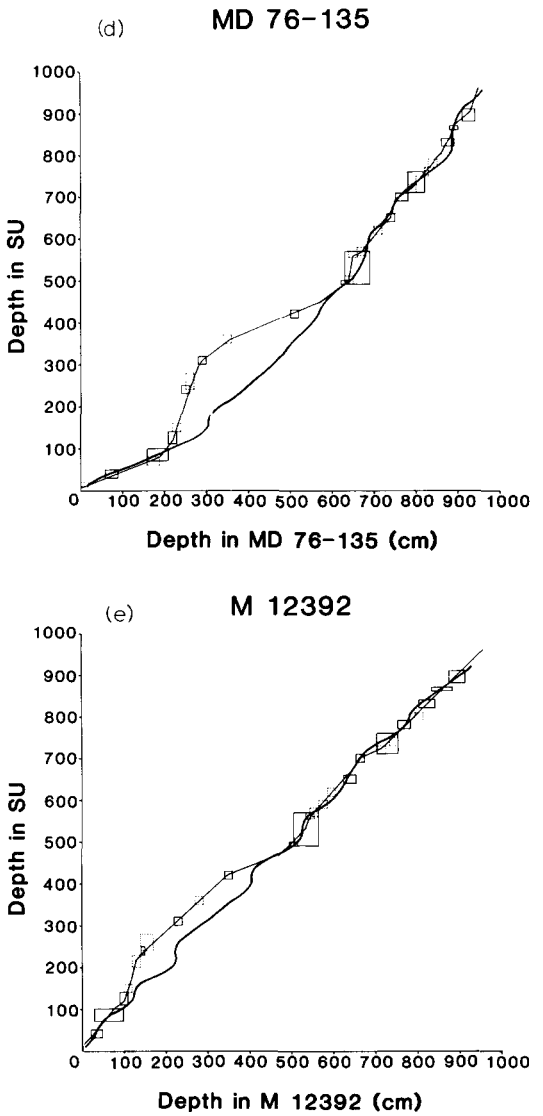

Fig.7. Comparison of graphic correlation results (light, straight line slope segments connecting the event boxes — minor events indicated by dashed boxes) with the inverse results (bold line) for the indicated record signals.

different interpretations in an anomalous section indicated in Fig.8a. Here, a single peak appears to show too much amplitude relative to other peaks in stage 2 (identified in Fig.8a) and was thus considered, in the graphical correlations, to signify the beginning of stage 3 as shown in Fig.8b. On the other hand, the adjacent down-core valley appears to be too deep to occur in stage 3. In the graphical correlations this deep valley is therefore considered an anomalous feature of stage 3. In the inverse correlation though, the valley

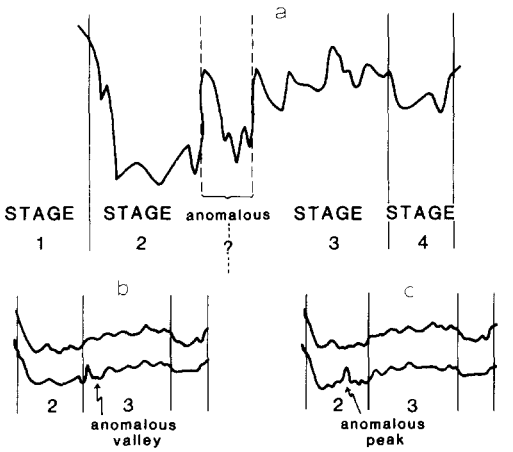

Fig.8. *a*. Portion of oxygen isotope signals showing area in which anomalous record blurs the boundary between stages 2 and 3 in core M12392. *b*. Interpretation adopted by workers using graphic correlation technique place anomaly as a deep valley in stage 3. *c*. Inverse method interpretation places anomaly as peak in stage 2.

is considered normal but the preceeding peak an anomalously high feature of stage 2 — not the beginning of stage 3 which is considered to begin immediately down-core of the valley (Fig.8c).

In either case, enough small scale features occur in the two cores to match each of the remaining features of stage 3 in the reference core. In M12392, these peaks seem to be approximately equally spaced so the two different interpretations end up being one peak out of phase relative to one another. This is seen in the superimposed mapping functions of the inverse vs. graphical correlation results, as a sharp divergence occurring at the position of disagreement followed by offset, but parallel lines which again converge at the mutually agreed upon beginning of stage 4. Either interpretation is acceptable as can be seen in Fig.7 (the graphical correlation interpretation would shift each of the peaks between 2 m and 4 m depth in M12392 over one peak to the right). The disagreement in stage 3 in MD76135 though, is not as clear and although the graphical correlate interpretation would again shift the peaks to the right it is by an irregular amount.

Table III summarizes the differences between the graphical and inverse correlation techniques based on the comparisons of standard depth units assigned to each sample in a core. For core Y7211 the mean difference is less than a centimeter with a standard error of about 1.5 cm. For cores V19-28, V19-30 and RC13-229 the differences are on the order of the sampling interval of each respective core. The mean differences between the two correlation techniques are rather large for cores MD76-135 and M12392 as would be expected from the previous discussion. If isotope stages 2 and 3 are not included in the average for these cores, the mean difference is also on the order of the sampling interval. Thus, it seems that the degree to which

TABLE III

Comparison of Shavian and inverse stratigraphies

Core	Average sediment rate (cm ka^{-1})	Mean diff.[1] (cm)	S.E. (mean) (cm)	Sampling interval of core (cm)
Y7211-2	12	0.57	1.4	7.2
V19-30	6	−5.9	0.6	3.3
V19-28	4	−9.8	1.6	11.6
RC13-229	2.2	−13.3	2.9	10.8
MD76-135	8	−40	5.0	10.0
M12392	6.5	−23	3.5	10.0

[1]Negative values indicate that graphical correlation placed events further down in core V19-29.

the isotope record can be correlated using these two stratigraphic techniques is limited by the sampling resolution of the cores themselves and to the extent to which similarities in the isotopic signal are globally or regionally uniform.

A composite isotope record

Given each sample from the cores studied and their standard depth assignments it is now possible to use these data to generate a generalized isotopic record. This record, ideally, has a higher signal to noise ratio than any individual core. Consider each core record as being composed of the real signal of isotopic change in the ocean plus a noise function. Also, assume that the noise functions all have the sample variance σ^2. If we average n cores, then the associated noise function will have variance σ^2/n. Such an average record, referred to here as a stack, was calculated using cores V19-29, V19-28, V19-30, Y7211, and RC13-229. Cores MD76-135 and M12393 were not used due to the uncertainty in the stratigraphic correlations as discussed above.

Before stacking, the isotopic values within a core were adjusted by subtracting the value midway between the most depleted interglacial event (usually stage 5e or stage 1) and the most enriched glacial event (usually stage 2). This value was usually equivalent to the data mean for a sample set except in the case of core Y7211. Stage 1 is partially lost in this core and the mean value for this core is biased towards enriched values. The scaling is intended to remove the effect of slight differences in the isotopic composition of the ocean's deep water. However, it assumes that the isotopic gradients between the South Atlantic, eastern equatorial Pacific and northeast Pacific have remained constant with time. By only removing a constant value within each core, the magnitude of change recorded at each sample location is unscaled and has equal weight in the stack record.

Composite isotope records were calculated using the correlations generated

by the graphical and inverse methods. Two stacking procedures were tried and both gave essentially identical results — the calculated composite record is independent of the correlation scheme used. The two stacking procedures used represent the extremes of the many possible strategies available. A stacked record was calculated by first interpolating the data for each core to a 0.5-cm interval (in standard depth units). Interpolating to this very fine interval assures that the original data values from each core will be included in the averaging process (0.5 cm is the lowest common denominator of all of the cores sampled) and that the average values will contain information from each core despite the irregular sampling of the various individual cores. The number of values averaged depends on the number of cores spanning the interval at which the average value is being calculated. The resulting stack is therefore calculated at 0.5 cm, but because many of the values used to calculate any one point may be interpolated, the resulting composite is relatively smooth.

The second stacking procedure utilizes only the data values and the assigned depths in the standard section. This procedure does not interpolate isotope values between real data points and is constructed by merging all scaled isotope values into one data series and sorting this file by assigned depth in the standard section. The stack is generated by averaging all isotope values which fall in a specified depth interval of the standard section. The depth intervals over which the averaging is done are adjacent but non-overlapping. The average value within a depth window is assigned the average depth of all points in the depth interval. The second stacking procedure, with a 10-cm window width, was used to calculate the composite records shown in Fig.9.

The two records are based on correlation of the same five cores using the graphical (Fig.9a) and inverse (Fig.9b) techniques and are essentially identical (correlation coefficient, $r^2 = 0.99$). These records have several important features. Many of the events used for the graphical correlation of the high resolution cores studied are well defined in these averaged records (cf. Fig.9; Table II). Even though five cores were averaged, these records show considerable variability that appears to be consistent from core to core. For example, marked variations of 0.2‰ in the average records are evident in glacial stages 6 and 3 (e.g. events 6.41, 6.42, 6.5, 6.6, 3.13, 3.31, 3.32). A short, intense glacial event in stage 7 is evident in the stacked records (7.4). Thus, the detailed variability observed in individual high sedimentation rate cores may indeed represent variations in the global climate system on a relatively short time scale. With the development of an accurate time scale for the late Pleistocene, this composite record could provide very valuable information about the short time scale variability of the Earth's climate.

CONCLUSIONS

(1) The results from the two stratigraphic correlation techniques show that very detailed correlations are possible. The resolution of this correlation

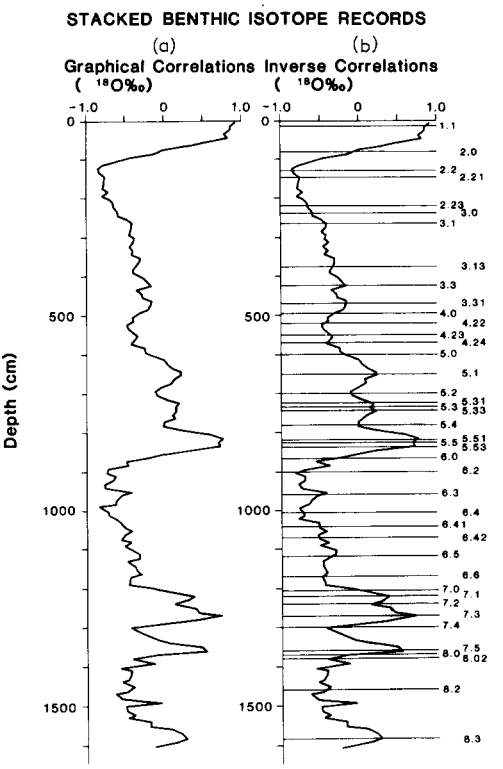

Fig.9. Results from averaging all benthic isotope records. a: graphic correlation average; b: inverse correlation average. Events used for graphical correlations shown on inverse stack.

is on the order of sampling intervals of sediment cores and thus regional differences in the oceanic response to changing global climates can be detected to a time resolution of at least 2000 to 4000 yrs. This approaches the mixing time of the ocean (~1000 yrs) which defines the limit of resolution of the oxygen isotopic global chronostratigraphy.

(2) Given these techniques and the standard isotopic curve developed here, any Pleistocene core with sufficient stratigraphic integrity and sampling resolution can be tied into this framework. Through this correlation the relative timing of change in other sediment components that monitor oceanographic and climatic change can be compared worldwide.

(3) An averaged composite isotopic record shows considerable variability on relatively short time scales indicating a measurable variability of even the high-frequency component of late Pleistocene isotopic (ice volume) change.

(4) Once an accurate time scale is applied to these data, their correlation to other Pleistocene records in the world ocean can be used to calculate highly precise estimates of interval accumulation rates for various sedimentary components.

(5) With such a time scale, we will also be able to better evaluate the

frequency dependence of climatic variability and how this may change for the various paleoceanographic indicators from place to place in the world ocean.

ACKNOWLEDGEMENTS

This study is a product of program SPECMAP — a multi-institutional program studying late Pleistocene climatic variability. This program is supported by NSF grants to Brown University (grant ATM80-18897), Columbia University, the University of Rhode Island and Oregon State University (grant ATM82-04127).

We wish to thank J. Duplessy who kindly provided data from core MD76-135 and Hank Streeter for his programming skills. Also Joe Morley and John Imbrie provided many useful suggestions.

REFERENCES

CLIMAP Project Members, 1976. The surface of the ice-age earth. Science, 191: 1131—1137.

CLIMAP Project Members, 1981. Seasonal reconstructions of the earth's surface at the last glacial maximum. Geol. Soc. Am., Map and Chart Series MC-36, Boulder, Colo.

Emiliani, C., 1955. Pleistocene temperatures. J. Geol., 63(6): 539—578.

Martinson, D.G., 1982. An inverse approach to signal correlation with applications to deep-sea stratigraphy and chronostratigraphy. Ph.D. Diss., Columbia University, New York, N.Y., 343 pp.

Martinson, D.G., Menke, W. and Stoffa, P., 1982. An inverse approach to signal correlation. J. Geophys. Res., 87: 4807—4818.

Mesolella, K.J., Mathews, R.K., Broecker, W.S. and Thurber, D.L., 1969. The astronomical theory of climate change: Barbados data. J. Geol., 77: 250—274.

Pisias, N.G., 1976. Late Quaternary sediment of the Panama Basin: Sedimentation rates, periodicities, and controls of carbonate and opal accumulation. In: R.M. Cline and J.D. Hays (Editors), Geol. Soc. Am. Mem., Boulder, Colo., 145: 375—392.

Shackleton, N.J., 1977. The oxygen isotope stratigraphic record of the late Pleistocene. Philos. Trans. R. Soc. London, Ser. B, 280: 169—182.

Shackleton, N.J. and Opdyke, N.D., 1973. Oxygen isotope and paleomagnetic stratigraphy of equatorial Pacific core V28-238: Oxygen isotope temperatures and ice volumes on a 10^5 and 10^6 year scale. Quat. Res., 3: 39—55.

Shackleton, N.J., Imbrie, J. and Hall, M.A., 1983. Oxygen and carbon isotope record of East Pacific core V19-30: Implication for the formation of deep water in the North Atlantic. Earth Planet. Sci. Lett., 65.

Shaw, A.B., 1964. Time in Stratigraphy. McGraw-Hill, New York, N.Y., 365 pp.

Shure, L. and Chave, A.D., 1983. An alternative approach to signal correlation. EOS, 64(18): 247 (abstract).